Supporting Information

Non-Conjugated Polymer Ligand: Stimulating Charge Transfer Towards Photocatalytic Selective Organic Transformation

Xing-Zu Ge,[a] Kun Wang,[a] Qiao-Ling Mo,[a] Yang Xiao,[a] Jia-Le Li,[a] Gao Wu,[a] Shu-Ran Xu,[a] Fang-Xing Xiao*[a, b]

a. College of Materials Science and Engineering, Fuzhou University, New Campus, Minhou, Fujian Province, 350108, China.

b. Fujian Science & Technology Innovation Laboratory for Optoelectronic Information of China, Fuzhou, Fujian 350108, P. R. China.

E-mail: fxxiao@fzu.edu.cn

Table of Contents

Experimental details

1.Preparation of Pd@PDDA NCs[S1]

400 μL PDDA (20% in water), 80 mL water, 200 μL 0.5 M NaOH and 300 μL Na_2PdCl_4 (20 mg/mL) were added into a beaker. After thoroughly mixed for 2 min, the mixed solution maintained at 100 ℃ for several minutes until the color of the solution changed to red and no further color change occurred. Through accurately control the reaction time and use an inverted culture dish covered on the beaker to avoid the reaction liquid vaporized rapidly.

2.Preparation of Pt@PDDA NCs

400 μL PDDA (20% in water), 80 mL water, 200 μL 0.5 M NaOH and 530 μL $H_2PtCl_6 \cdot 6H_20$ (20 mg/mL) were added into a beaker. After thoroughly mixed for 2 min, the mixed solution maintained at 100 ℃ for several minutes until the color of the solution changed to red and no further color change occurred. Through accurately control the reaction time and use an inverted culture dish covered on the beaker to avoid the reaction liquid vaporized rapidly.

3.Preparation of $Zn_{0.5}Cd_{0.5}S$ nanowires[S2]

1 mmol of $ZnCl_2$ and 1 mmol of $CdCl_2 \cdot 2.5H_2O$ were added into Teflon-lined stainless-steel autoclaves together with 2 mmol of $(NH_4)_2S$. Then the autoclaves were filled with 20 wt% ethylenediamine aqueous solution up to 80% of the capacity (50 mL). The autoclaves were maintained at 180 ℃ for 48 h and then cooled down naturally to room temperature. The precipitates were filtered and washed with DI H_2O and ethanol successively. The final products were dried in vacuum at 80 ℃ for 2 h.

4.Preparation of photoelectrodes

PEC measurements were carried out on electrochemical workstations (CHI 660E & Gamary Interface 1000 E) in a conventional three-electrode quartz cell using 0.5 M Na_2SO_4 aqueous solution (100 mL, 0.5 M, pH = 6.69) as the electrolyte. A Pt plate was used as the counter electrode, Ag/AgCl electrode was used as the reference electrode, and the samples coated on fluorine-dope tin oxide (FTO) glass were utilized as the

working electrodes.[S3] Working electrodes were prepared on FTO glass that was cleaned by sonication in ethanol for 30 min and dried at 353 K. The boundary of FTO glass was protected using scotch tape. The 10 mg sample was dispersed in 1 mL of ethyl alcohol absolute by sonication to get slurry which was uniformly spread onto the pretreated FTO glass. After drying in the air, the Scotch tape was unstuck, and the uncoated part of the electrode was isolated with nail polish. The exposed area of the working electrode was 1 cm^2.

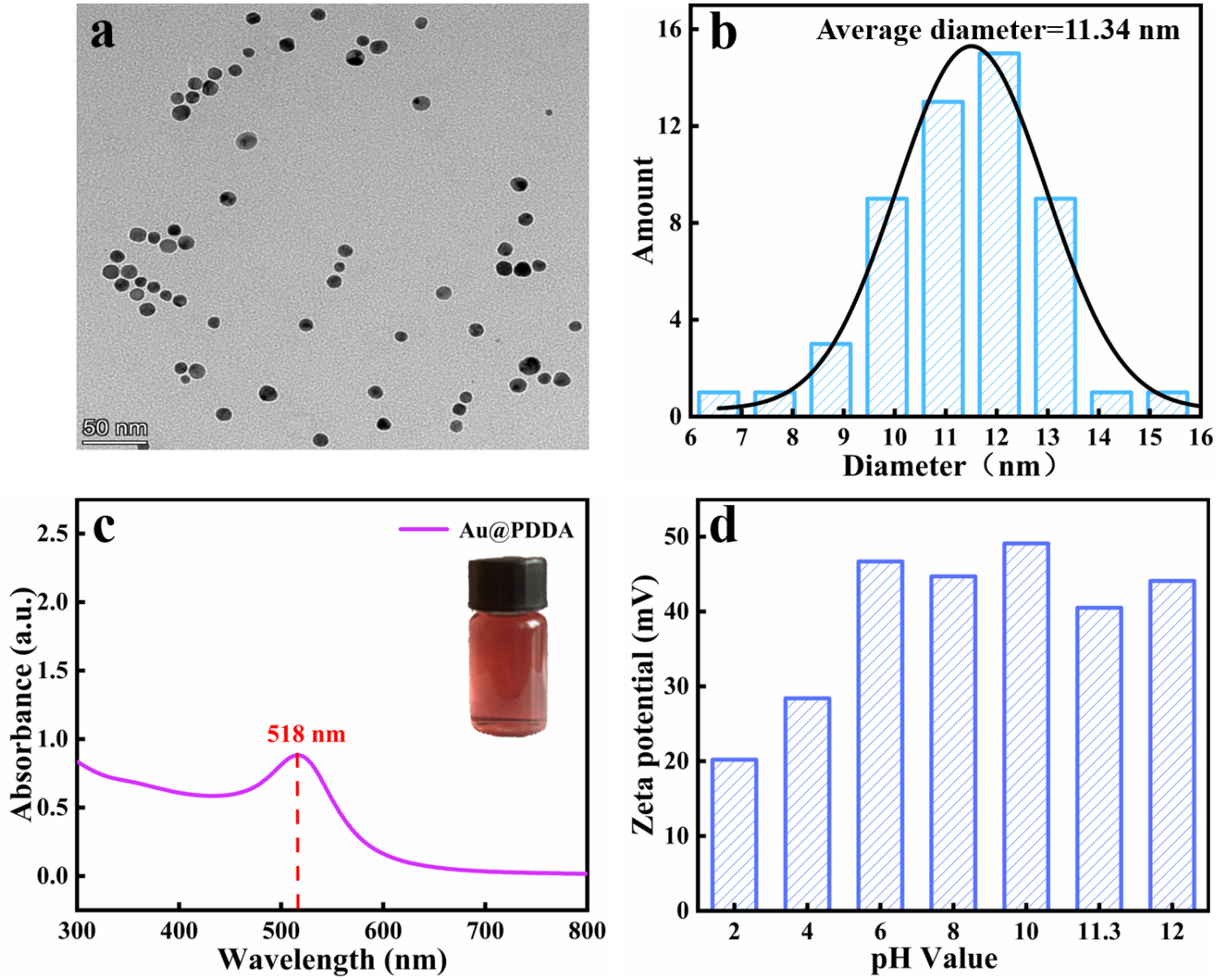

Figure S1. (a) TEM image of Au@PDDA NCs with (b) size distribution histogram, (c) UV-vis absorption spectrum of Au@PDDA NCs colloidal solution and (d) zeta potentials of Au@PDDA NCs as a function of pH value.

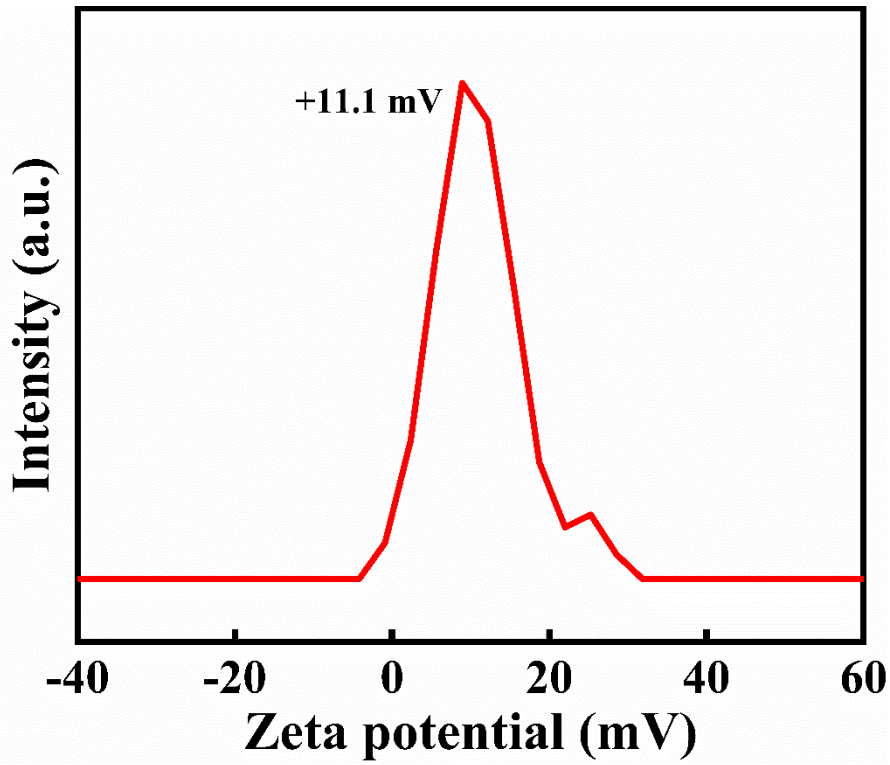

Figure S2. Zeta potential of CdS.

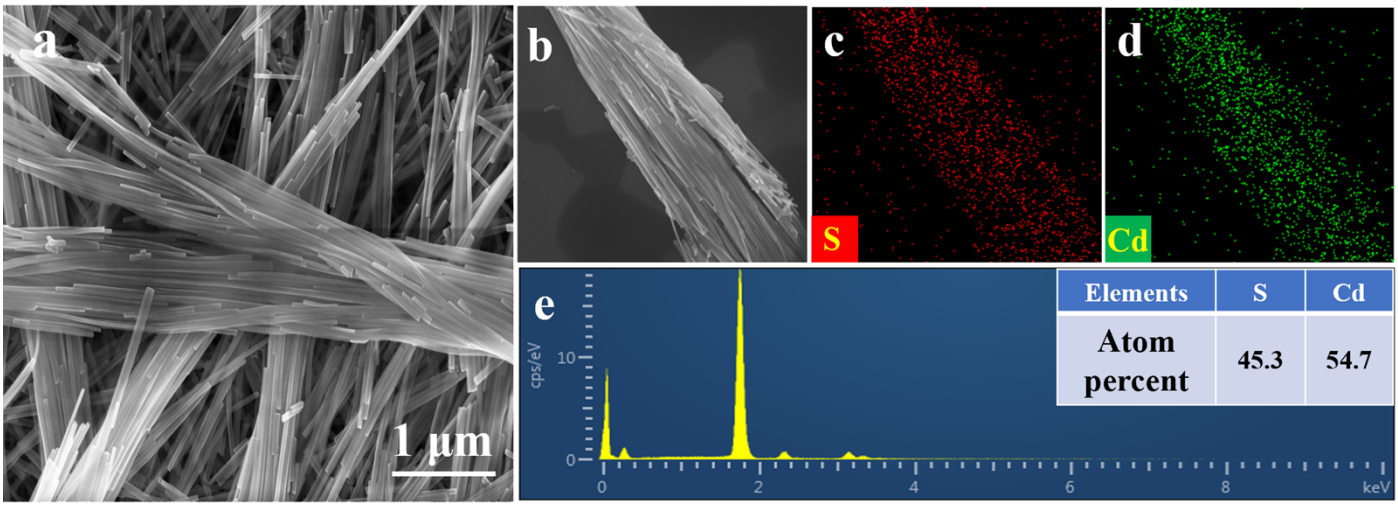

Figure S3. (a & b) SEM images of CdS NWs with (c-d) elemental mapping and (e) EDS results.

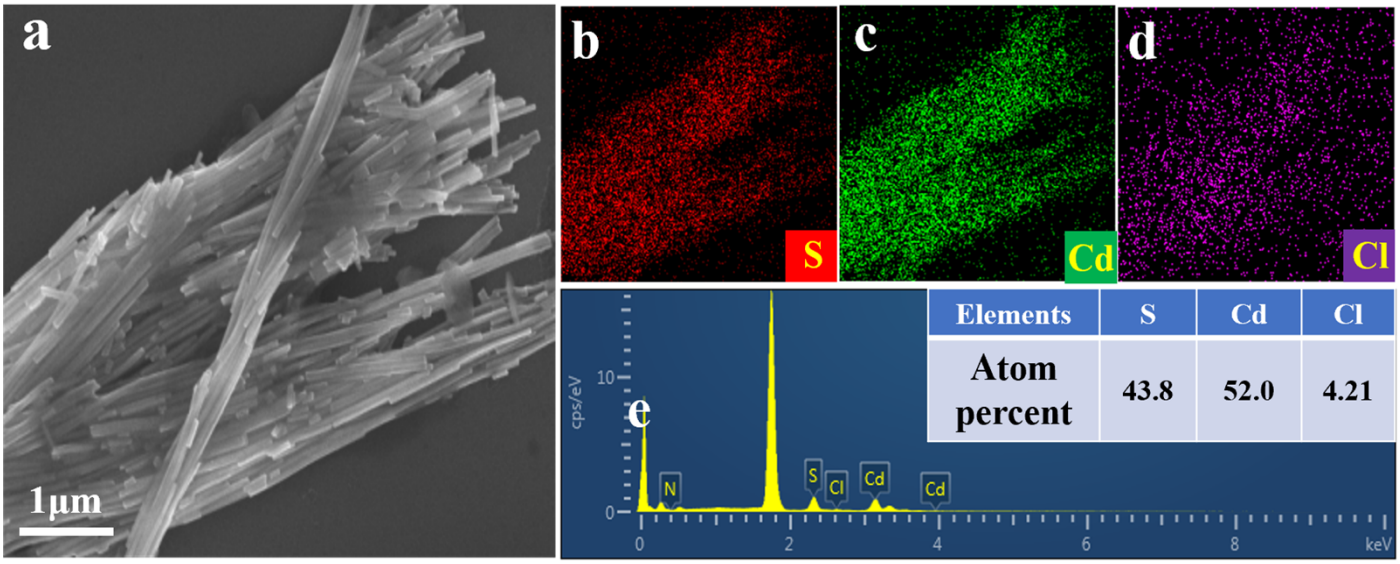

Figure S4. (a) SEM image of PDDA/CdS with (b-d) elemental mapping and (e) EDS results.

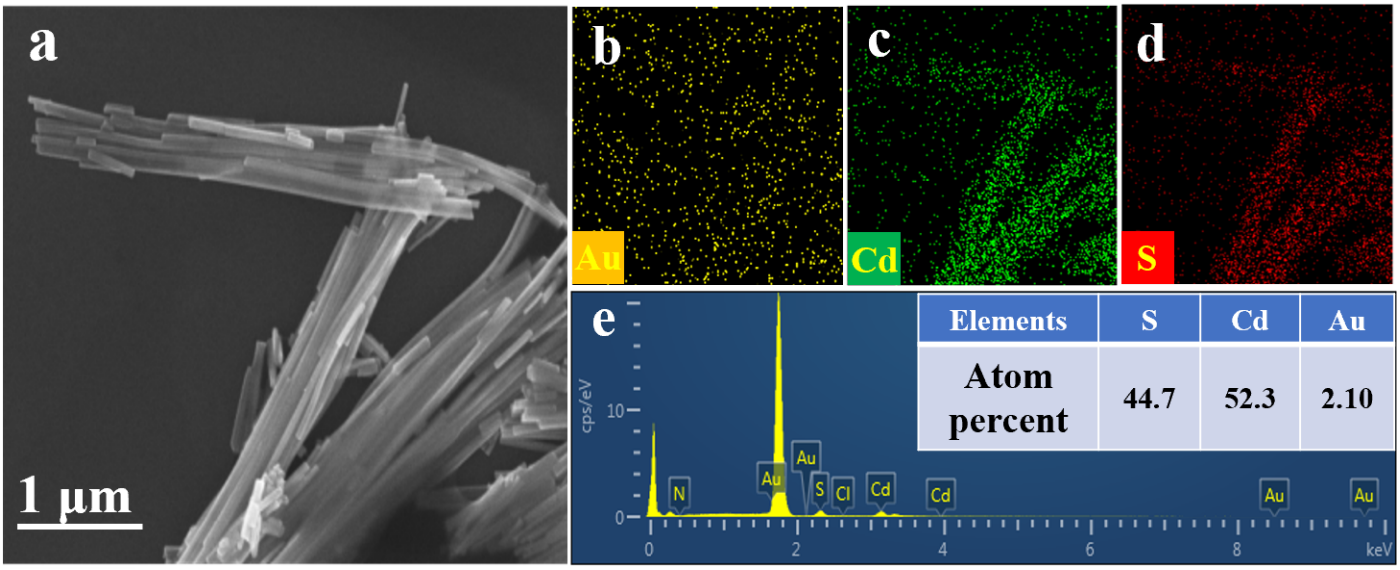

Figure S5. (a) SEM image of Au@PDDA/CdS heterostructure with (b-d) elemental mapping and (e) EDS results.

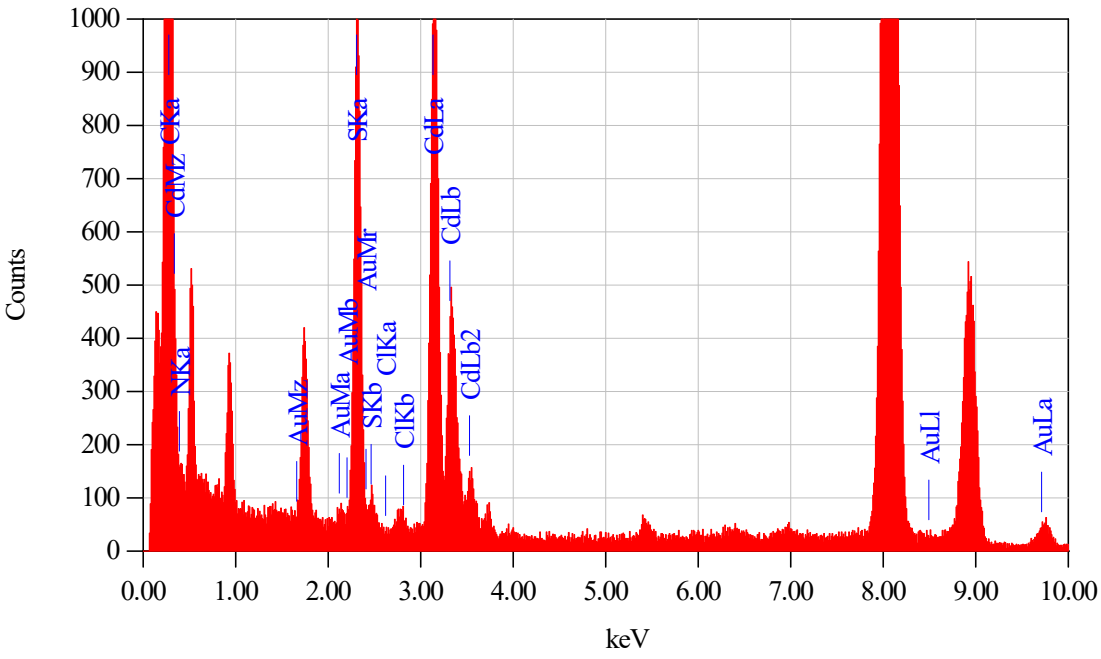

Figure S6. EDS result of 2%Au@PDDA/CdS heterostructure.

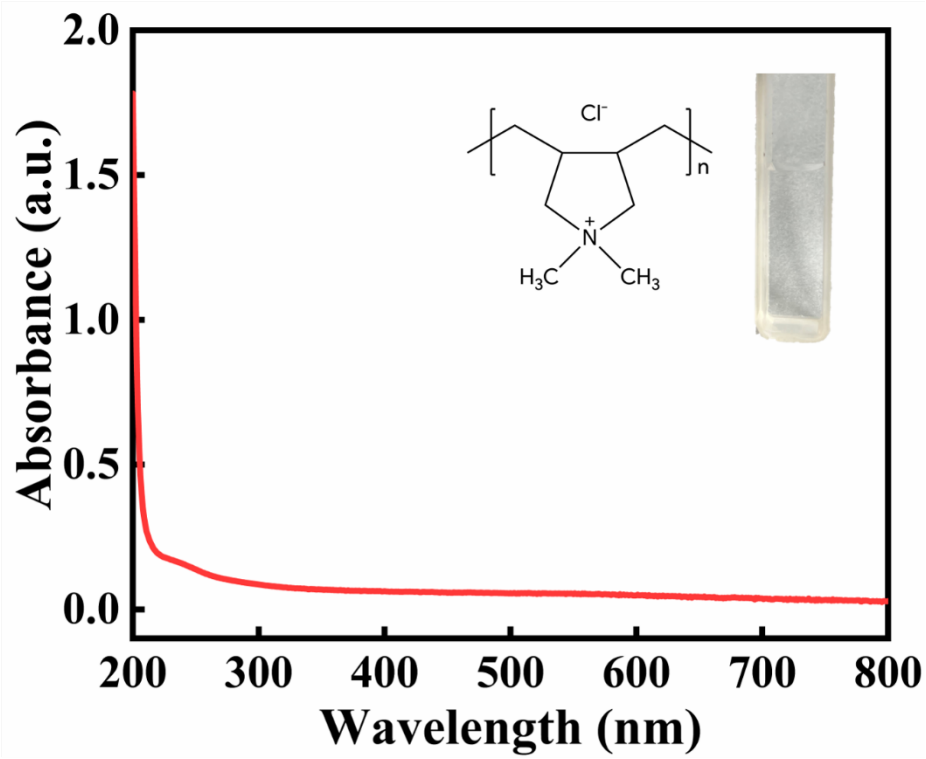

Figure S7. UV-vis absorption spectrum of PDDA aqueous solution with molecular structure in the inset.

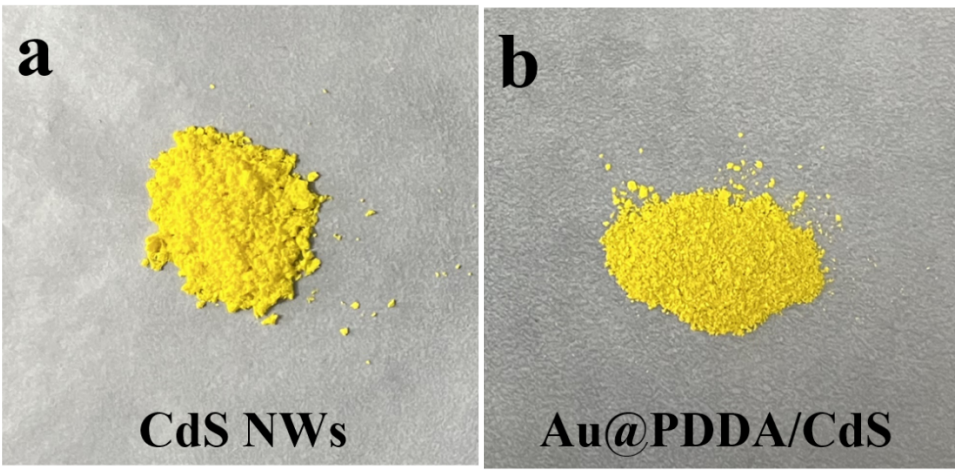

Figure S8. Sample colors of (a) CdS NWs and (b) 2%Au@PDDA/CdS heteostructure.

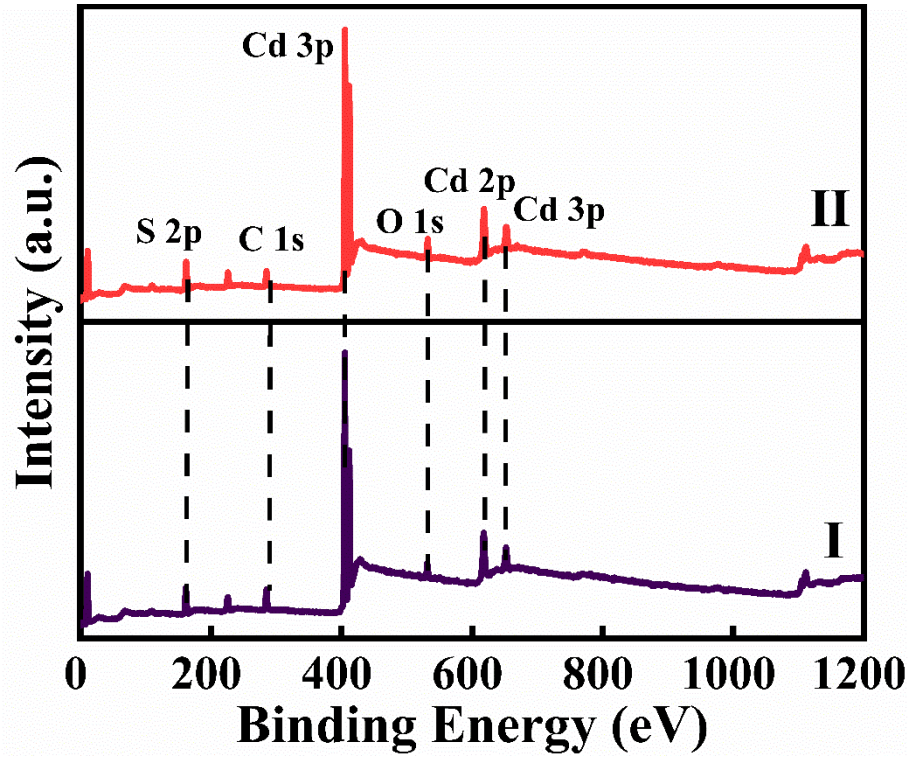

Figure S9. Survey spectra of (I) CdS NWs and (II) 2%Au@PDDA/CdS heterostructure.

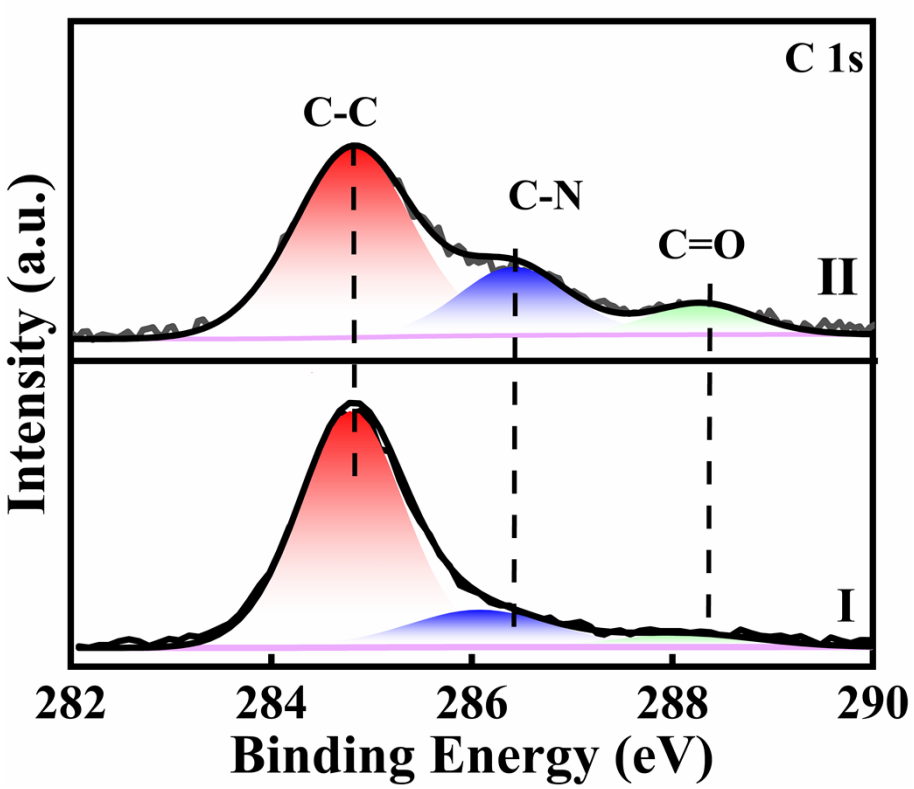

Figure S10. High-resolution C 1s spectra of (I) CdS NWs and (II) 2%Au@PDDA/CdS heterostructure.

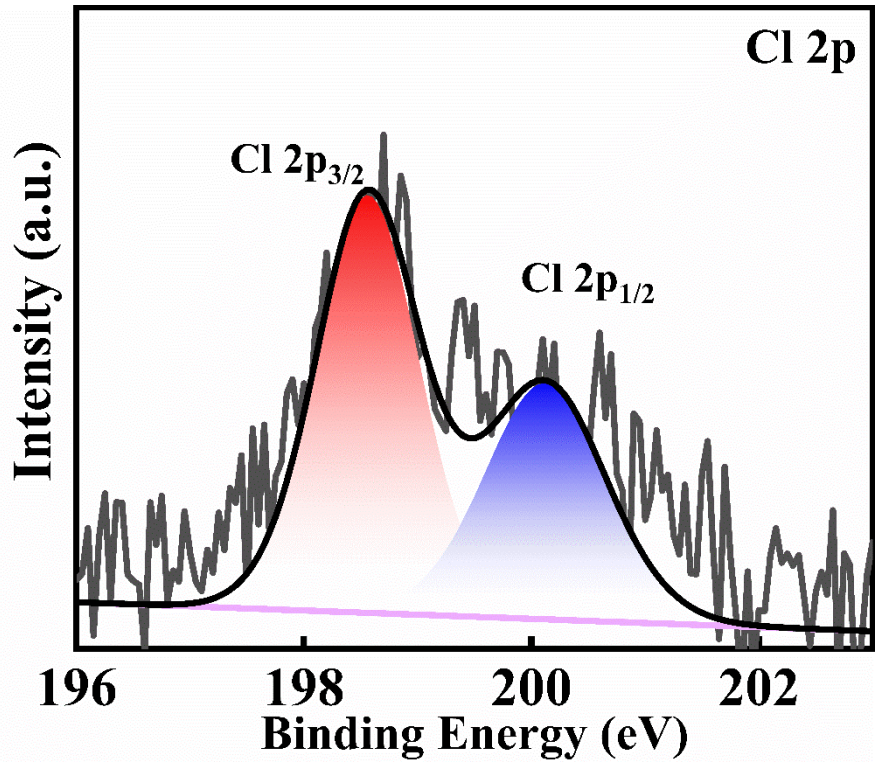

Figure S11. High-resolution Cl 2p spectrum of 2%Au@PDDA/CdS heterostructure.

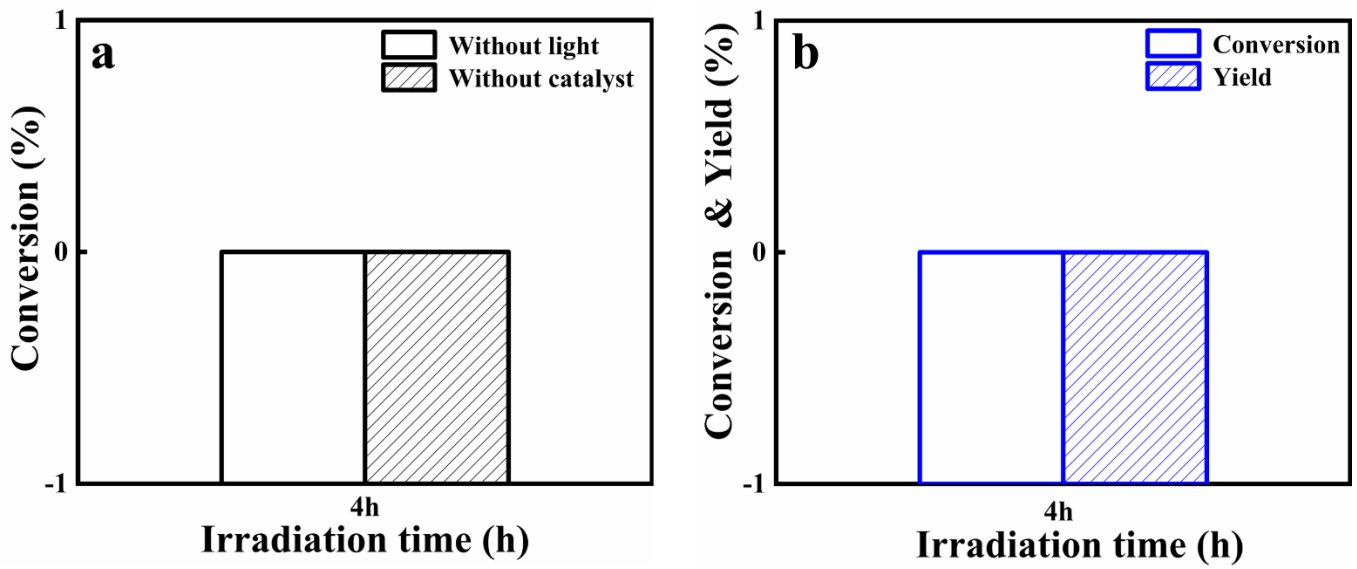

Figure S12. (a) Blank experiments for photocatalytic selective oxidation of benzyl alcohol without light irradiation or without adding photocatalyst, and (b) photoactivity of Au@PDDA NCs toward selective oxidation of benzyl alcohol under visible light irradiation.s

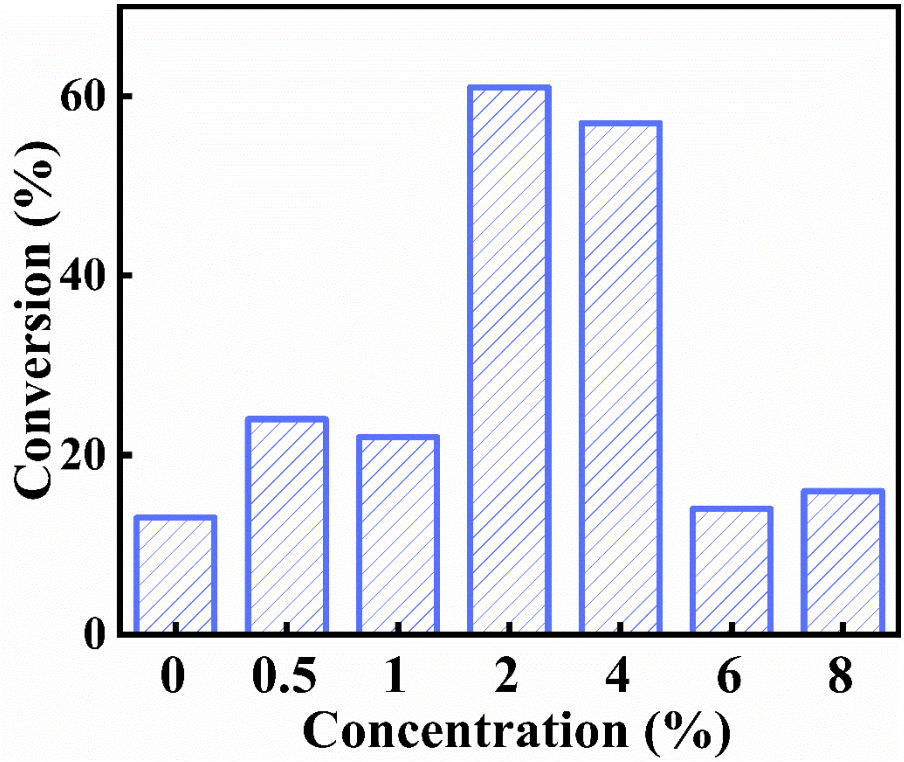

Figure S13. Photoactivities of Au@PDDA/CdS with different loading percentage of Au@PDDA NCs.

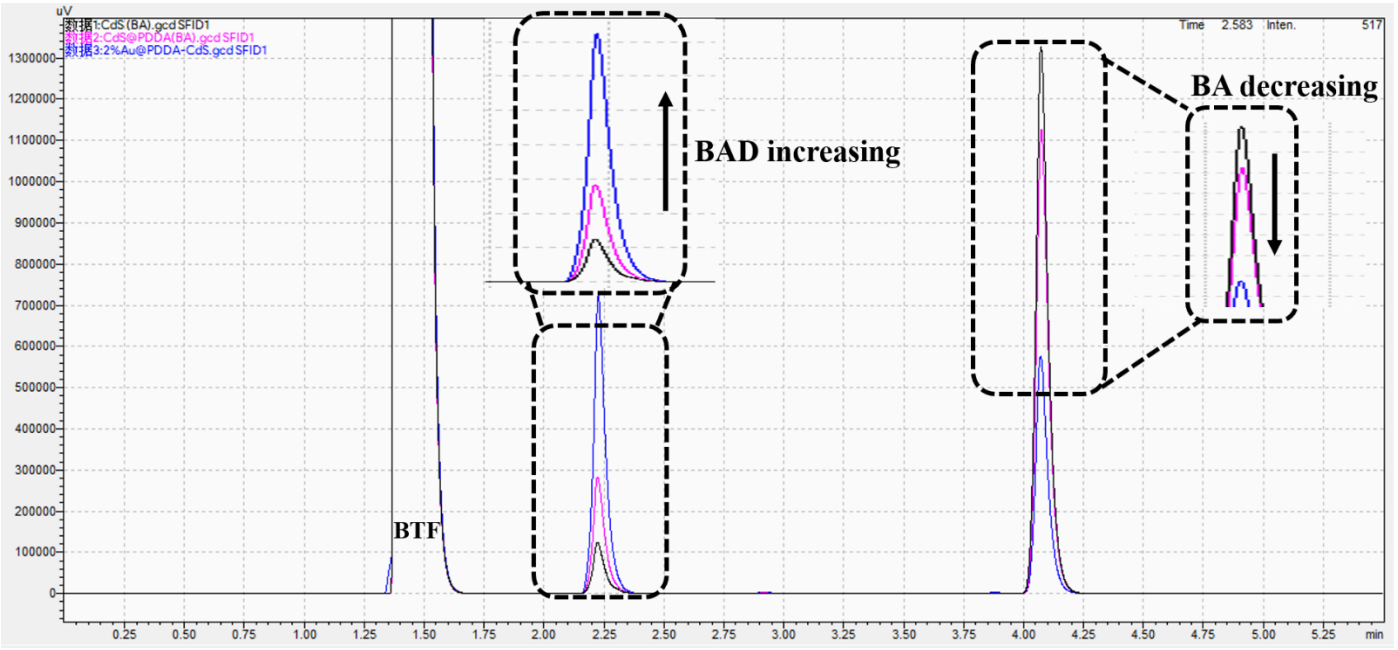

Figure S14. GC spectrum illustrating selective oxidation of BA to BAD over CdS NWs, PDDA/CdS and 2%Au@PDDA/CdS under visible light irradiation (λ>420 nm). The peaks from left to right correspond to BTF, BAD, and BA, respectively.

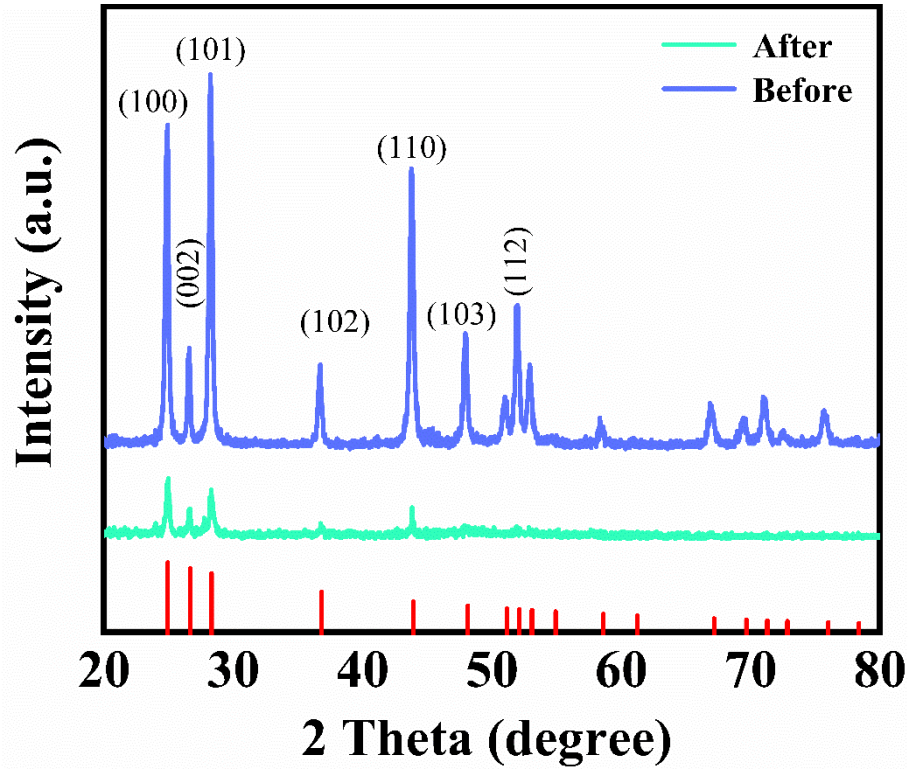

Figure S15. XRD patterns of 2%Au@PDDA/CdS heterostructure before and after five cyclic photooxidation reaction.

`

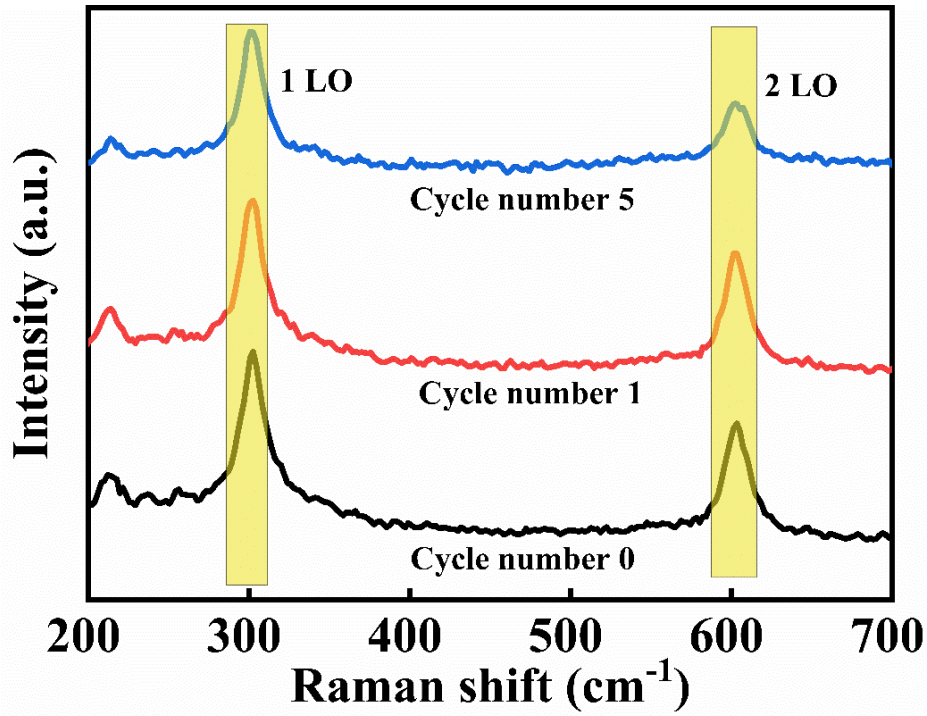

Figure S16. Raman spectra of Au@PDDA/CdS heterostructure after cyclic reaction.

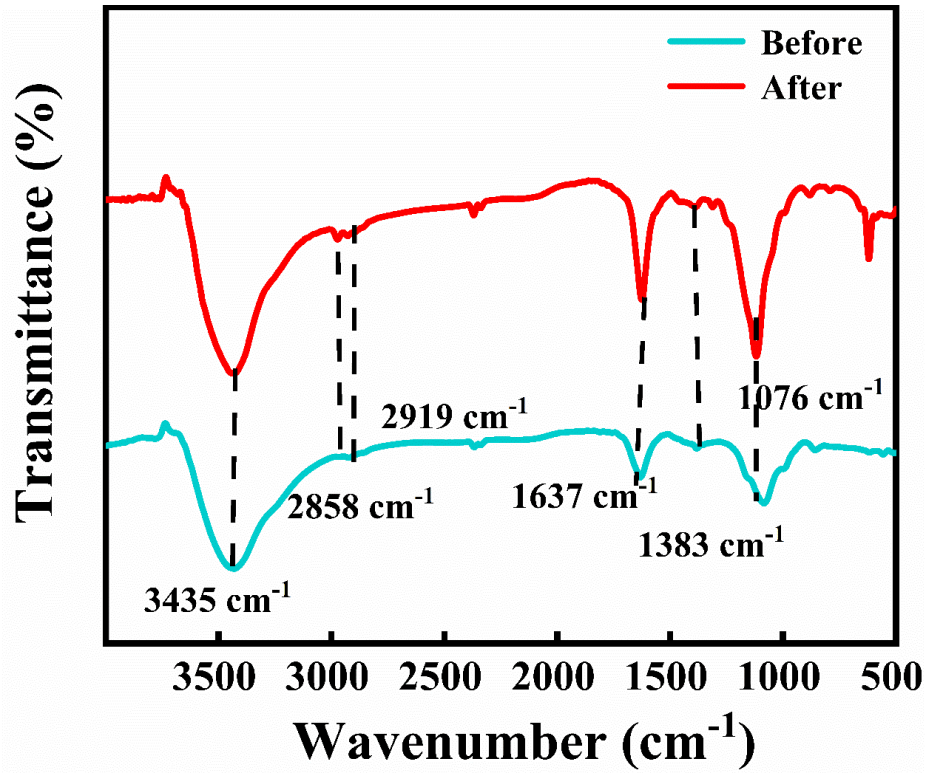

Figure S17. FIIR spectra of Au@PDDA/CdS heterostructure before and after cyclic reaction.

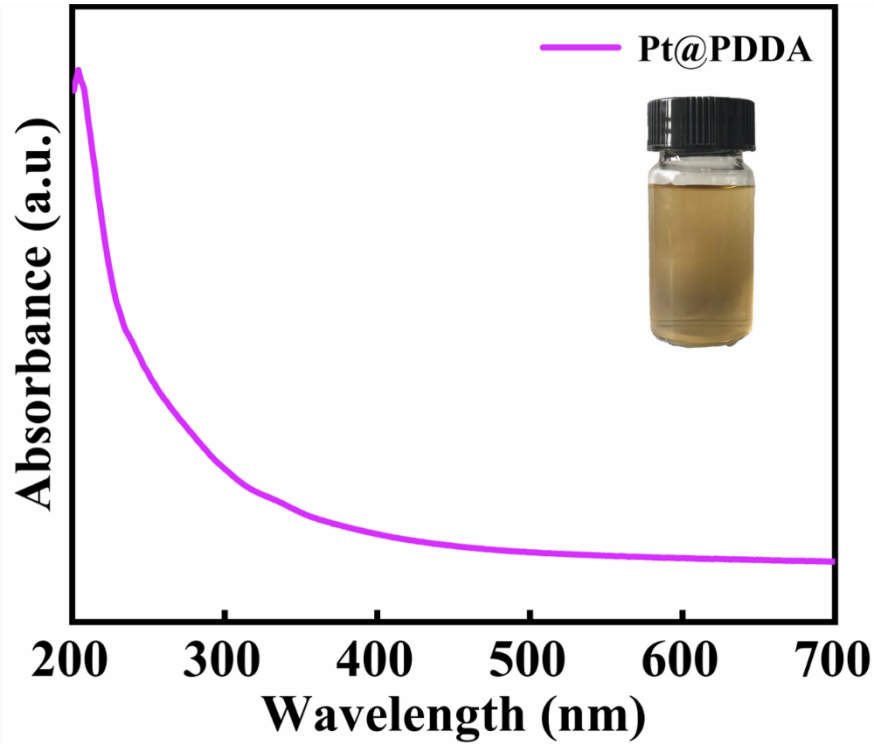

Figure S18. UV-vis absorption spectrum of Pt@PDDA NCs colloidal solution.

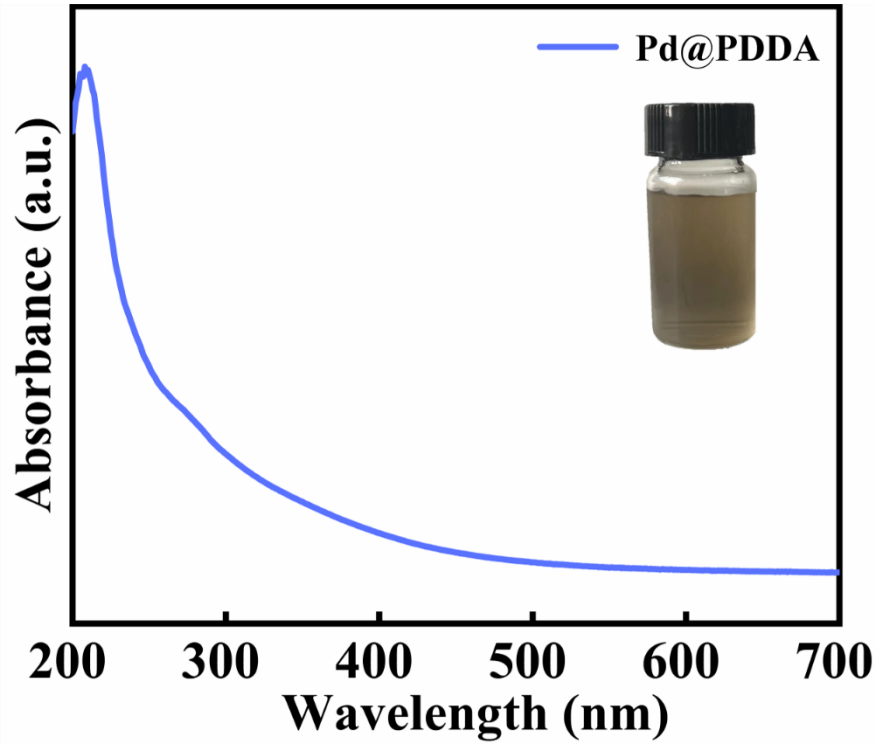

Figure S19. UV-vis absorption spectrum of Pd@PDDA NCs colloidal solution.

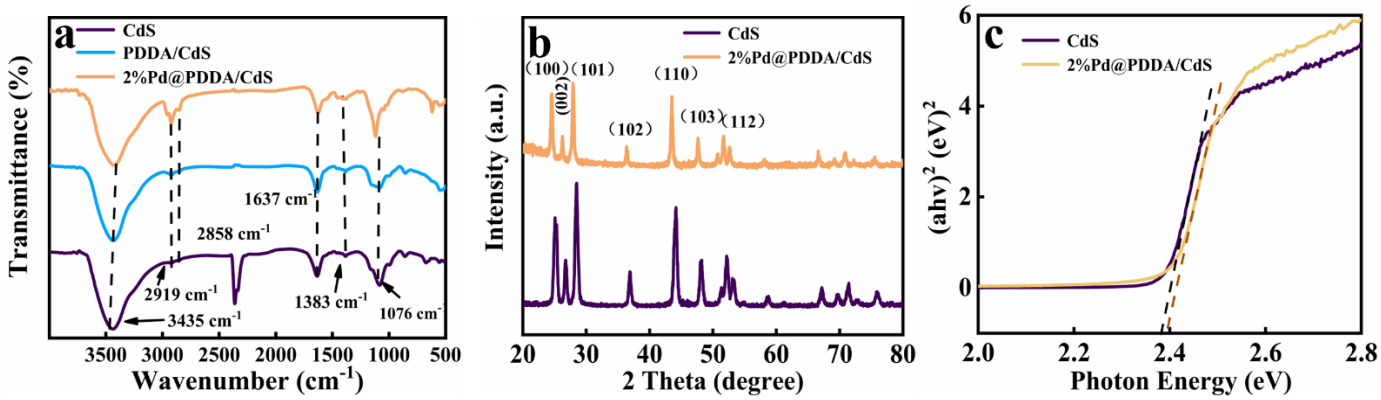

Figure S20. (a) FTIR spectra of pristine CdS and 2%Pd@PDDA/CdS heterostructure, (b) XRD patterns of pristine CdS and 2%Pd@PDDA/CdS heterostructure along with (c) transformed plots calculated based on the Kubelka– Munk function vs. the energy of light.

Note: As displayed in **Fig. S20a**, the characteristic peaks at 1076 and 3435 cm^{-1} in the FTIR spectrum of CdS NWs are assignable to the stretching and bending vibration modes of O–H groups. Notably, no new peak was observed in the FTIR spectrum of Pd@PDDA/CdS heterostructure with respect to that of blank CdS NWs, which is primarily due to the low loading amount of Pd@PDDA NCs on the CdS NWs. As shown in **Fig. S20b**, XRD results reveal that the primary peaks correspond to CdS with the hexagonal phase (JCPDS no. 41-1049). However, no diffraction peak of Pd@PDDA NCs can be discerned in the XRD result of Pd@PDDA/CdS heterostructure, and this is mainly ascribed to the ultralow deposition amount of Pd@PDDA NCs. The transformed plots based on the Kubelka–Munk function vs. the photon energy are provided in **Fig. S20c**, by which bandgaps of CdS NWs and Pd@PDDA/CdS heterostructure were roughly determined to be 2.4 eV, respectively. This result implies that self-assembly of Pd@PDDA NCs on the CdS NWs did not influence the absorption band edge of Pd@PDDA/CdS heterostructure.

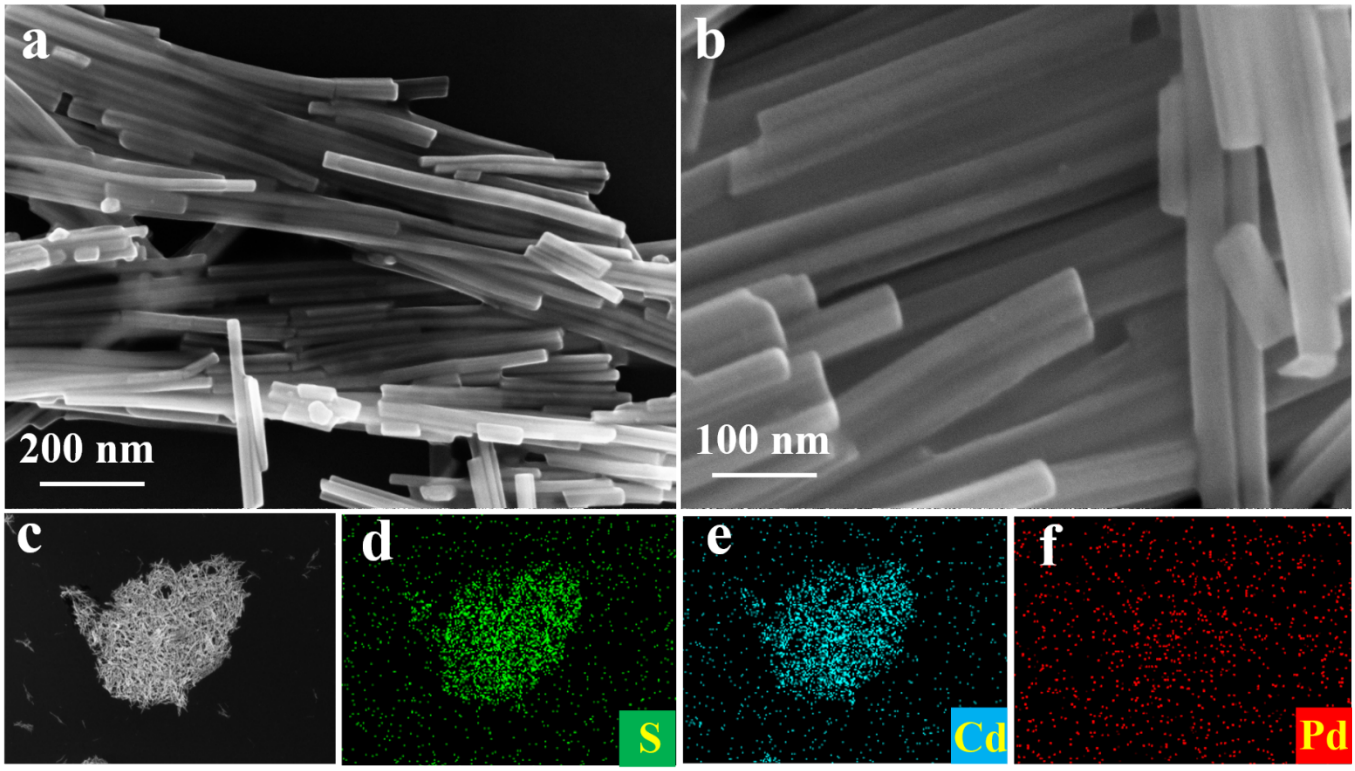

Figure S21. (a-c) SEM images and (d-f) elemental mapping results of 2%Pd@PDDA/CdS heterostructure.

Note: Fig. S21(a-c) show the morphology of Pd@PDDA/CdS heterostructure. in which 1D morphology is well maintained. **Fig. S21(d-f)** show the mapping results of Pd@PDDA/CdS heterostructure, which persuasively evidence the deposition of Pd@PDDA NCs on the CdS NWs.

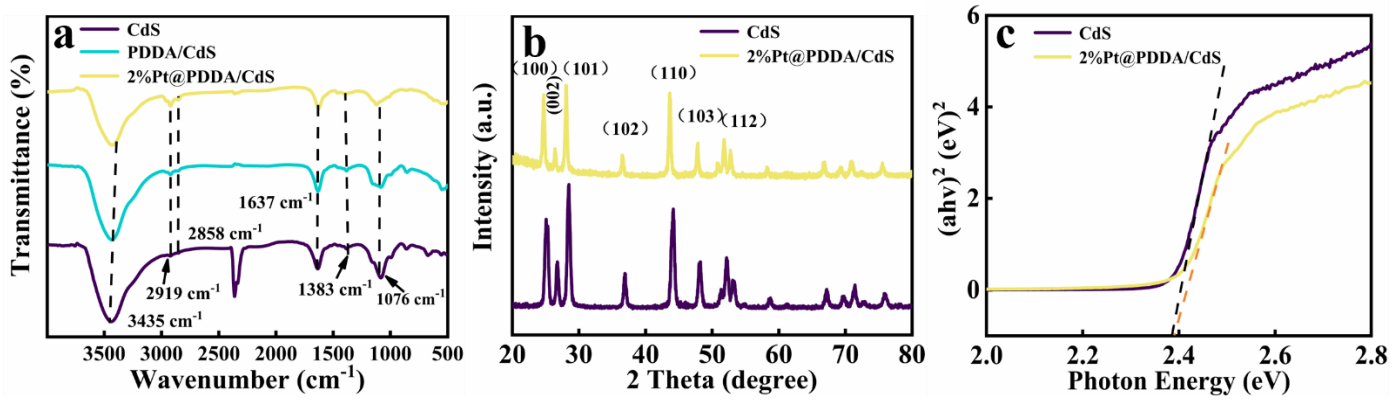

Figure S22. (a) FTIR spectra of pristine CdS NWs and 2%Pt@PDDA/CdS heterostructure, (b) XRD patterns of pristine CdS NWs and 2%Pt@PDDA/CdS heterostructure along with (c) transformed plots calculated based on the Kubelka– Munk function vs. the energy of light.

Note: Similar results were observed in the characterizations of Pt@PDDA/CdS heterostructure. As displayed in **Fig. S22a,** no new peak was observed in the FTIR spectrum of Pt@PDDA/CdS heterostructure with respect to CdS NWs, and this is primarily due to the low loading amount of Pd@PDDA NCs on the CdS NWs. As shown in **Fig. S22b**, no diffraction peak of Pd@PDDA NCs can be discerned in the XRD result of Pt@PDDA/CdS heterostructure. The transformed plots based on the Kubelka–Munk function vs. the photon energy are provided in **Fig. S22c**, by which bandgaps of CdS NWs and Pt@PDDA/CdS heterostructure were roughly determined to be 2.4 eV, respectively. This result implies that self-assembly of Pt@PDDA NCs on the CdS NWs did not influence the light absorption band edge of Pt@PDDA/CdS heterostructure.

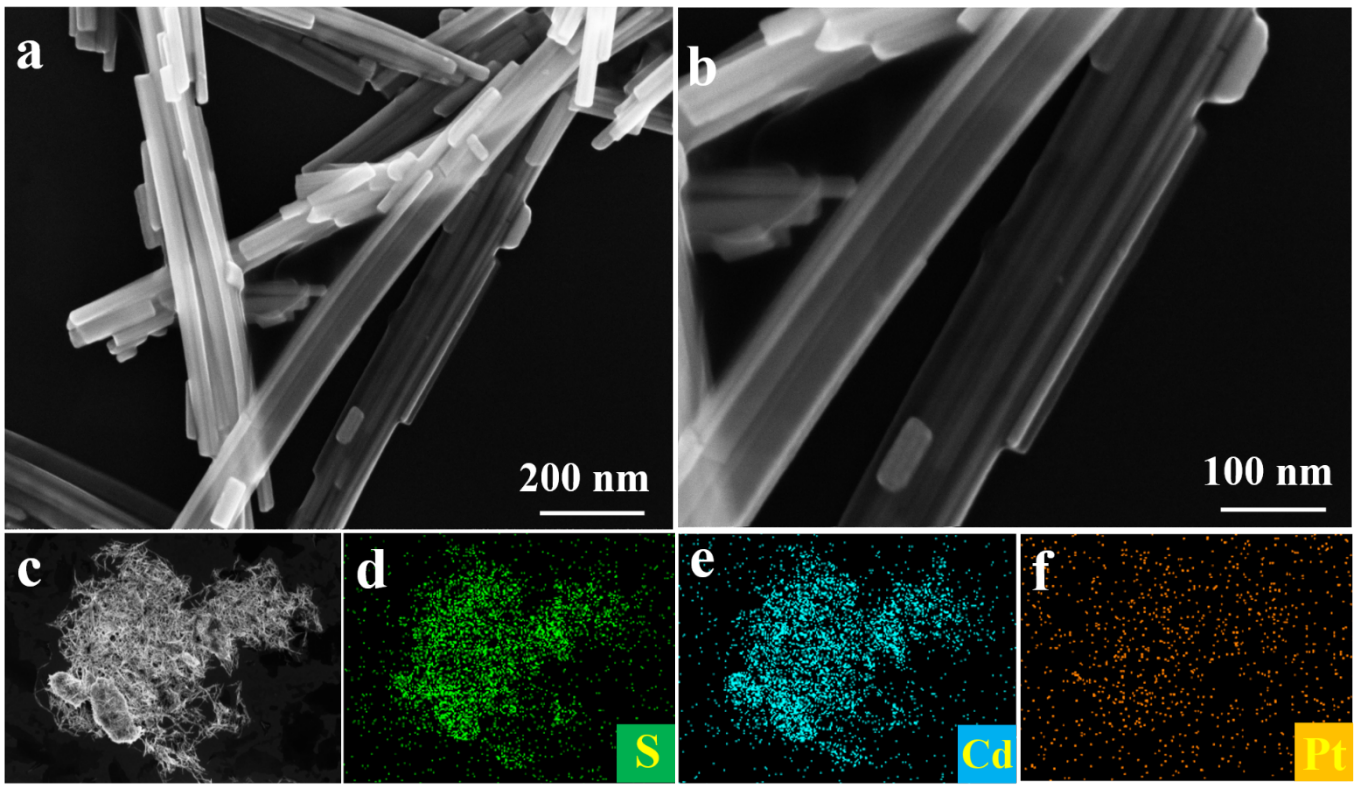

Figure S23. (a-c) SEM images and (d-f) elemental mapping results of 2%Pt@PDDA/CdS heterostructure.

Note: Fig. S23(a-c) demonstrate the morphology of Pt@PDDA/CdS heterostructure. in which 1D nanostructure is remained. **Fig. S23(d-f)** exhibit the mapping results of Pt@PDDA/CdS heterostructure, which confirm the successful deposition of Pt@PDDA NCs on the CdS NWs.

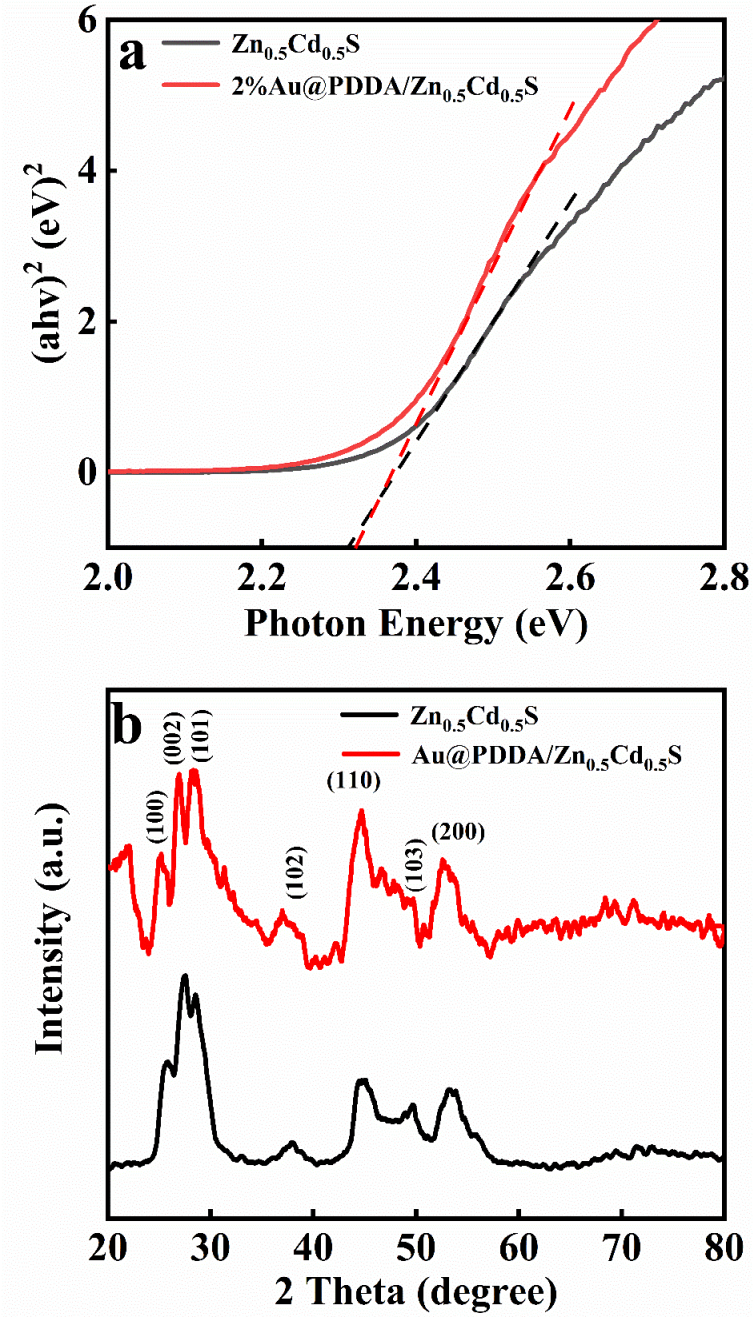

Figure S24. (a) Transformed plots calculated based on the Kubelka–Munk function vs. the energy of light, (b) XRD patterns of pristine $Zn_{0.5}Cd_{0.5}S$ NWs and 2%Au@PDDA/$Zn_{0.5}Cd_{0.5}S$ heterostructure.

Note: As shown in **Fig. S24a**, bandgaps of $Zn_{0.5}Cd_{0.5}S$ NWs and 2%Au@PDDA/$Zn_{0.5}Cd_{0.5}S$ heterostructure were determined to be 2.31, and, 2.32 eV, respectively. The results suggest that absorption band edge of $Zn_{0.5}Cd_{0.5}S$ NWs is not affected by Au@PDDA NCs deposition. XRD patterns of samples are shown in **Fig. S24b,** all of which are assigned to the wurtzite hexagonal $Zn_{0.5}Cd_{0.5}S$ NWs. However, no diffraction peak of Au@PDDA NCs can be discerned in the XRD result of 2%Au@PDDA/$Zn_{0.5}Cd_{0.5}S$ heterostructure, and this is mainly ascribed to the ultralow deposition amount of Au@PDDA NCs.

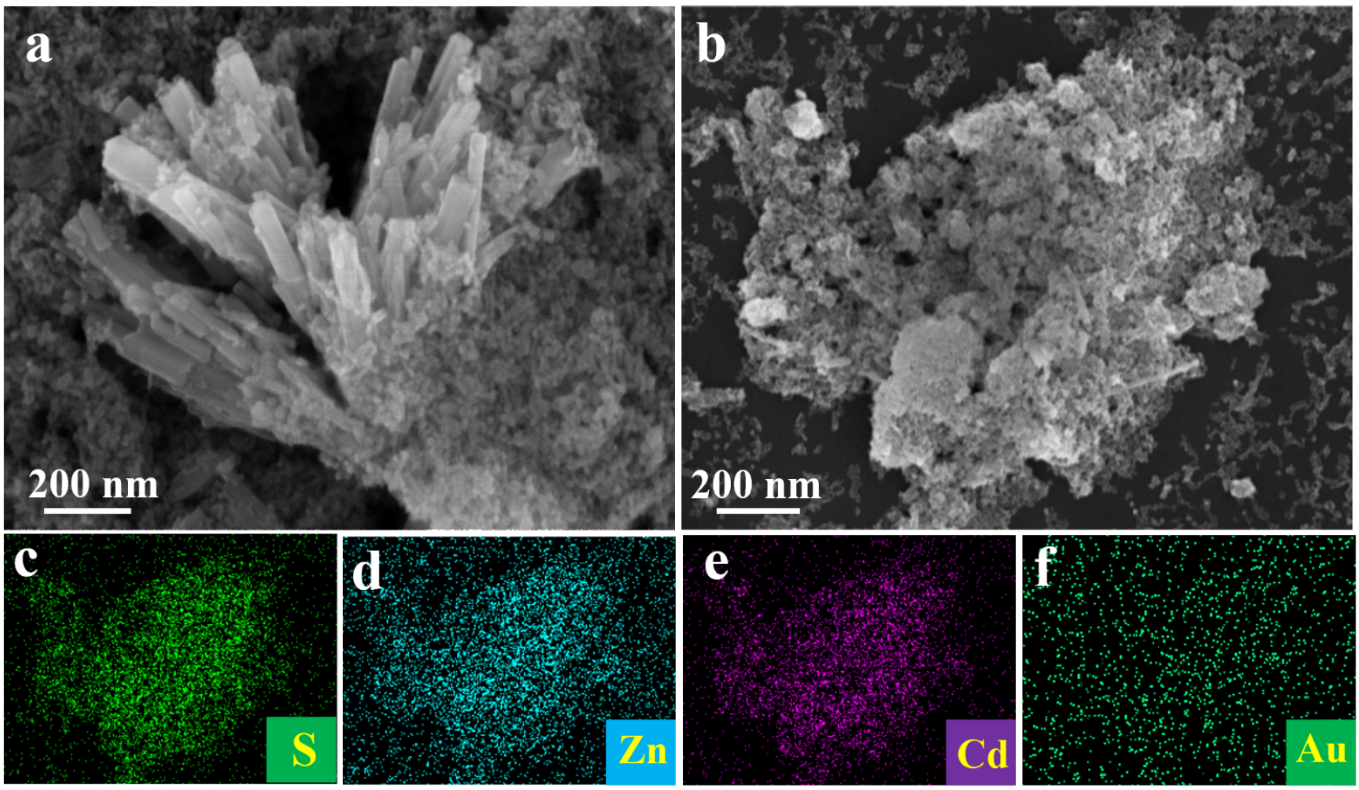

Figure S25. (a & b) SEM images of Au@PDDA/$Zn_{0.5}Cd_{0.5}S$ heterostructure, and (c-f) elemental mapping results of 2%Au@PDDA/$Zn_{0.5}Cd_{0.5}S$ heterostructure.

Note: Fig. S25(a & b) show the morphology of Au@PDDA/$Zn_{0.5}Cd_{0.5}S$ heterostructure, in which 1D morphology is maintained. **Fig. S25(c-f)** show the mapping results of Au@PDDA/$Zn_{0.5}Cd_{0.5}S$ heterostructure, which evidences the deposition of Au@PDDA NCs.

Table S1. Peak position with corresponding functional groups.

Peak position (cm^{-1})	Chemical bond
3435	$-NH_2$, $-OH$[S4]
2919&2858	$-CH_3$
1627	-COOH, $-NH_2$[S5]
1383	$-CH_3$
1076	-C-N-

Table S2. Specific surface area, pore volume and pore size of blank CdS NWs and 2.0%Au@PDDA/CdS heterostructure.

Samples	S_{BET} (m^2 /g)[a]	Total pore volume (cm^3 /g)[b]	Average pore size (nm)[c]
CdS	31.0107	0.053819	6.94202
Au@PDDA/CdS	22.4591	0.043134	7.68222

a BET surface area is calculated from the linear part of BET plots.
b Single point total pore volume of the pores at $P/P_0 = 0.95$.
c Adsorption average pore width (4V/A by BET).

Table S3. Chemical bond species vs. B.E. for different samples.

Elements	CdS NWs	Au@PDDA/CdS	Chemical bond species	Ref.
Cd $3d_{5/2}$	404.9	405.2	Cd^{2+}	S6
Cd $3d_{3/2}$	411,6	412.0	Cd^{2+}	
S $2p_{3/2}$	161.3	161.5	S^{2-}	S7
S $2p_{1/2}$	162.4	162.7	S^{2-}	
C 1s	284.8	284.8	C-C	
C 1s	286.4	286.6	C-O	S8
C 1s	288.0	288.2	C=O	
Cl $2p_{3/2}$	N.D.	198.5	Cl^-	S9
Cl $2p_{1/2}$	N.D.	200.1	Cl^-	
Au $4f_{7/2}$	N.D.	84.9	Au^0	S10
Au $4f_{5/2}$	N.D.	88.4	Au^0	

N.D.: Not Detected

Table S4. Fitted EIS results of different photoanodes under visible light irradiation (λ>420 nm).

Photoanodes	**Rs /ohm**	**Rct /ohm**	**CPE /(F·cm^{-2})**
CdS	10.42	14540	5.489E-5
PDDA/CdS	10.17	12330	5.549E-5
Au@PDDA/CdS	9.423	10150	5.373E-5

References

S1. H. Chen, Y. Wang, Y. Wang, S. Dong and E. Wang, Polymer, 2006, **47**, 763-766.

S2. Q. Nie, Q. Yuan, Q. Wang and Z. Xu, J. Mater. Sci., 2004, **39**, 5611-5612.

S3. X.-C. Dai, M.-H. Huang, Y.-B. Li, T. Li, B.-B. Zhang, Y. He, G. Xiao and F.-X. Xiao, J. Mater. Chem. A, 2019, **7**, 2741-2753.

S4. X. Y. Fu, Y. B. Li, M. H. Huang, T. Li, X. C. Dai, S. Hou, Z. Q. Wei and F. X. Xiao, Inorg. Chem., 2020, **59**, 2562-2574.

S5. H. Liang, B.-J. Liu, B. Tang, S.-C. Zhu, S. Li, X.-Z. Ge, J.-L. Li, J.-R. Zhu and F.-X. Xiao, ACS Catal., 2022, **12**, 4216-4226.

S6. J. You, L. Wang, W. Bao, A. Yan and R. Guo, J. Mater. Sci., 2021, **56**, 6732-6744.

S7. R. K. Chava, J. Y. Do and M. Kang, ACS Sustain. Chem. Eng., 2018, **6**, 6445-6457.

S8. Q.-L. Mo, X. Lin, Z.-Q. Wei, X.-C. Dai, S. Hou, T. Li and F.-X. Xiao, J. Mater. Chem. A, 2020, **8**, 16392-16404.

S9. S. Y. Yu, W. E. O'Grady, D. E. Ramaker and P. M. Natishan, J. Electrochem. Soc., 2000, **147**, 2952.

S10. D. C. Lim, I. Lopez-Salido, R. Dietsche, M. Bubek and Y. D. Kim, Angew. Chem. Int. Ed. Engl., 2006, **45**, 2413-2415.